Development and Uncertainty Characterization of Rotating 3D Velocimetry using a Single Plenoptic Camera

M. Moaven, A. Gururaj, Z. P. Tan[‡], S. Morris, B. S. Thurow [1*], V. Raghav [2*]

Auburn University, Department of Aerospace Engineering, Auburn, AL, USA

[1*] thurow@auburn.edu

[2*] raghav@auburn.edu

Abstract

Rotating 3D velocimetry (R3DV) is a single-camera PIV technique designed to track the evolution of flow over a rotor in the rotating reference frame. A high-speed (stationary) plenoptic camera capable of 3D imaging captures the motion of particles within the volume of interest through a revolving mirror from the central hub of a hydrodynamic rotor facility, a by-product being an undesired image rotation. R3DV employs a calibration method adapted for rotation such that during MART reconstruction, voxels are mapped to pixel coordinates based on the mirror's instantaneous azimuthal position. Interpolation of calibration polynomial coefficients using a fitted Fourier series is performed to bypass the need to physically calibrate volumes corresponding to each fine azimuth angle. Reprojection error associated with calibration is calculated on average to be less than 0.6 of a pixel. Experimental uncertainty of cross-correlated 3D/3C vector fields is quantified by comparing vectors obtained from imaging quiescent flow via a rotating mirror to an idealized model based purely on rotational kinematics. The uncertainty shows no dependency on azimuth angle while amounting to approximately less than 0.21 voxels per timestep in the in-plane directions and correspondingly 1.7 voxels in the radial direction, both comparable to previously established uncertainty estimations for single-camera plenoptic PIV.

1 Motivation

There exist countless unsteady fluid dynamics problems involving rotation - an action tending to give rise to highly 3D flow features; however, diagnostics of such flows have traditionally been constrained to phase-averaged PIV and time-resolved experiments within a stationary frame of reference (Mulleners et al. (2012); Percin and Oudheusden (2015)). Recording the three-dimensional evolution of rotating flows through time is paramount to the success of aerodynamicists in understanding and predicting flows such as that around a helicopter rotor.

Rotating 3D velocimetry (R3DV) is a technique capable of continuously tracking and reconstructing time-resolved 3D flow over a rotor within the rotating frame of reference. Images are captured via a 45° inclined mirror that is rotating in conjunction with the wing, thereby transporting the rotating field of view containing the flow as it evolves above the wing through a 90° turn and towards a stationary camera (see Fig. 1). Herein lies the cornerstone of R3DV - a high-speed plenoptic camera capable of 3D imaging. The feature that sets a plenoptic camera apart from a conventional camera is an array of microlenses placed between the camera sensor and main lens. This simple modification enables incoming light rays to be encoded based on their angle of incidence with the main lens. As a result, plenoptic images can be decoded to resolve volumetric information (Fahringer et al. (2015)) and whilst 3D flow-field measurements have traditionally relied on multi-camera configurations, the plenoptic camera can be the sole imaging device in a 3D-PIV experiment. This provides a crucial advantage in an optically restricted environment such as that of the current R3DV implementation. For a more comprehensive discussion of the R3DV technique as well as details of the experimental configuration, the authors would like to point the reader to "Rotating three-dimensional velocimetry" by Gururaj et al. (2021).

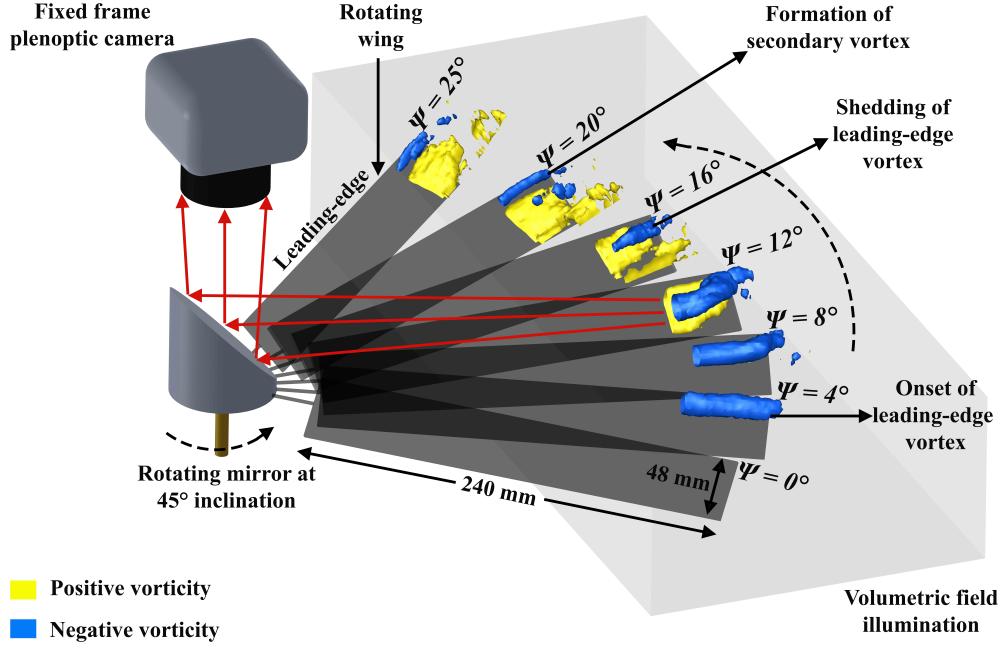[‡]Currently at: National Yang Ming Chiao Tung University

Figure 1: R3DV setup schematic including isosurfaces of vorticity (not to scale)

The purpose of this paper is to address unique challenges that arise from imaging with the configuration used in R3DV, namely the development of a rotational calibration method and quantification of uncertainty with a potential dependency on rotation. It can be deduced based on intuition that imaging with a stationary camera via a rotating mirror results in a continuously rotating image. Fig. 2 illustrates this effect by showing a calibration plate mounted at the position of the wing starting from a position (Fig. 2(a)) and undergoing an approximately 40° azimuthal rotation (ψ) (Fig. 2(b)), resulting in the camera viewing the plate as having been rotated by the same angle ψ. Ideally, the rotation should be rectified prior to cross-correlation such that imaged flow particles are not seen as experiencing a false rotation. A simple 2D rotation matrix on plenoptic images would be inappropriate in addressing this as a raw image contains thousands of microlens sub-images meaning any such operation would impose an artificial rotation on the microlens array. As such, an existing volumetric calibration method was adapted to a rotating field of view in order to seamlessly incorporate rotation into camera calibration such that Fig. 2(b) is transformed to Fig. 2(c) to match the orientation of Fig. 2(a). Section 3 discusses the details of this method as well as results from an error analysis including a comparison to plenoptic calibration in a stationary frame benchtop setup. In PIV experiments designed to examine the growth and formation of a leading-edge vortex (LEV) around a 45° pitch wing, R3DV was shown to give qualitatively agreeable results with existing literature. Of course, the viability of a novel PIV implementation cannot be assumed based solely on qualitative observation. As such, images of quiescent flow were recorded via the rotating mirror without the presence of a wing - the impetus being to compare resulting vector fields of the perceived rotating flow to a model based on rotational kinematics in order to quantify the uncertainty of the method. With the imaged volume rotating through a wide range of angles, a potential dependency of uncertainty on azimuth angle must simultaneously be investigated. Results of the uncertainty analysis and a comparison to single camera plenoptic-PIV in the stationary frame are presented in Section 4.

2 Rotating 3D Velocimetry

2.1 Technique

A typical tomographic or plenoptic-PIV experiment begins with recording images of a volume of illuminated particles seeding the flow of interest (Fig. 3). A fundamental step specific to processing of plenoptic images involves determining the projected microlens positions on the image sensor. Subsequent steps for both tomo-PIV and plenoptic-PIV are based on the same principles of calibrating the volume with respect to the camera,
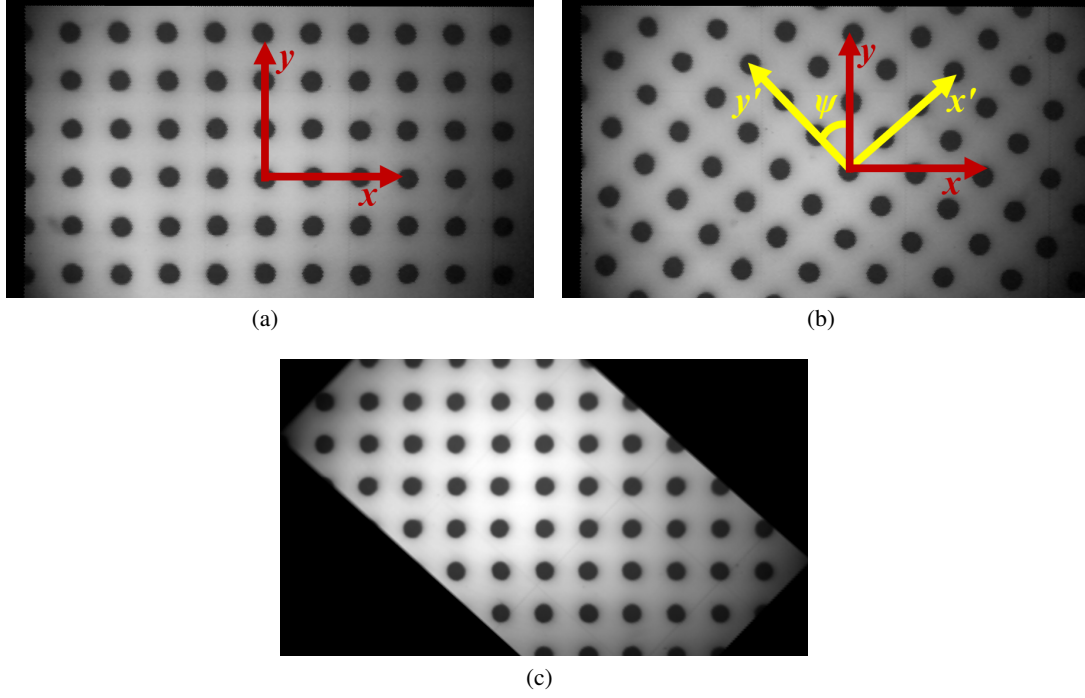
Figure 2: Rotated field of view (b) resulting from mirror rotation of angle ψ rectified using rotational calibration to generate image (c) with feature point coordinates consistent with that of image (a)

using said calibration to reconstruct the volume of interest, and finally cross-correlating consecutive images to yield vector fields of particle displacements. As alluded to in the previous section, the unique nature of R3DV's rotating field of view is addressed within the volumetric calibration step. Here, a rotational calibration technique establishes a relationship between the image and the volume while taking into account its orientation. Applying this calibration during volumetric reconstruction generates an intensity field that is dependent on the azimuth angle of the mirror at that instant meaning any rotation of the field of view as a consequence of looking through the rotating mirror is eliminated. As a visual aid for the aforementioned quiescent flow experiments, this results in the camera adopting the perspective of the mirror such that particle images theoretically undergo only translation.

2.2   Setup

The configuration shown in Fig. 1 is an inverted schematic of the arrangement used in this work, with the mirror and wing assembly contained in a 1.2 m × 1.2 m × 1.2 m acrylic water tank and an encoder incorporated to track the mirror's azimuth angle. The plenoptic camera assembly is composed of a 4096 × 2304 pixel resolution Phantom VEO 4k 990L camera and a Modular Plenoptic Adaptor (Tan et al. (2019)) that houses a 471 × 362 microlens array, an optical relay system, as well as a 200 mm main imaging lens. The calibration plate was held in place by a mounting wing consisting of evenly spaced holes to position the plate at 10.16 mm increments in the depth direction. During uncertainty measurement acquisition, water in the tank was seeded with fluorescent PMMA rhodamine particles at a density of approximately 0.04 particles per microlens (ppm). Volume illumination was provided by a LaVision LED-Flashlight 300 positioned normal to one of the tank's sides and a 52 mm Tiffen Orange 21 lens filter was used to enhance the signal-to-noise ratio of particle images.

2.3   Data Acquisition and Processing Parameters

The calibration plate was imaged at 9 consecutive positions on the mounting wing, covering a depth of 81.28 mm. The wingless experiments of section 4 designed for uncertainty analysis were performed for two volumes corresponding to two different locations on the wing used in the flow visualization experiments
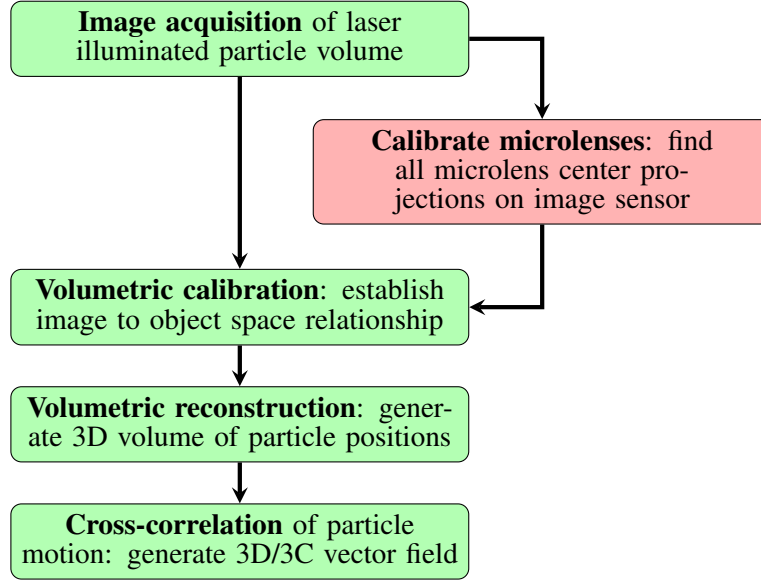
Figure 3: General roadmap of tomographic and conventional plenoptic-PIV (left, green) versus additional step exclusive to plenoptic-PIV (right, red) (detailed tomographic-PIV workflow in Elsinga et al. (2006))

of Gururaj et al. (2021), across the same range of azimuth angles. Volume 1 denotes the volume placing the focal plane near the tip of the wing while volume 2 was centered slightly inboard. Experiments for each volume were repeated with three different rotation rates (approximately 1, 3, and 5 RPM) at an image acquisition rate of 200 fps. The theoretical field of view at the focal plane was calculated to be 68×38.2 mm and 60.7×34 mm for volume 1 and volume 2, respectively. Seven iterations of a plenoptic-adapted MART algorithm were used to reconstruct volumes at a grid resolution of 8 vox/mm. The cross-correlation algorithm used here is based on a multi-pass 3D (VODIM) scheme. Cubic window sizes of [64, 48, 40, 40] voxels in each dimension with overlaps of 75% were applied to generate vector fields of size $52 \times 28 \times 76$ for volume 1 and $44 \times 23 \times 76$ for volume 2, with vector spacings of 1.25 mm.

3 Rotational Volumetric Calibration

This section details the calibration technique developed for application in a rotating volume – the necessity of which arises when a field of view is relayed via a rotating mirror to a stationary camera thus causing the image to exhibit in-plane rotation (Fig. 2).

In a conventional (stationary) field of view, our group employs a technique known as direct light-field calibration (DLFC) to relate a plenoptic image to object space (Hall et al. (2018)). Here, images of a calibration pattern at known depths relative to the focal plane are captured, covering a total depth that typically encloses the volume of interest. These images are then decoded into perspective views with each perspective representing a discrete location (u, v) on the aperture plane. A generic third-order polynomial is used as a mapping function to pair every location on the microlens plane (s, t) to its corresponding location in object space (x, y, z) via each perspective:

$$s = P(x, y, z, u, v) = a_{s_0} + a_{s_1}x + a_{s_2}y + a_{s_3}z + a_{s_4}u + a_{s_5}v + a_{s_6}x^2 + a_{s_7}xy + \cdots + a_{s_{55}}v^3$$
$$t = P(x, y, z, u, v) = a_{t_0} + a_{t_1}x + a_{t_2}y + a_{t_3}z + a_{t_4}u + a_{t_5}v + a_{t_6}x^2 + a_{t_7}xy + \cdots + a_{t_{55}}v^3 \tag{1}$$

Polynomial variables are stored in a matrix $\mathbf{A}$ where each row corresponds to a calibration feature point at a unique depth and perspective view. Subsequently, the coefficients of Eq. 1 are calculated by method of least-squares, $\mathbf{a_s} = \mathbf{A}/\mathbf{s}$ and $\mathbf{a_t} = \mathbf{A}/\mathbf{t}$, where $\mathbf{s}$ and $\mathbf{t}$ represent vectors of s and t positions. The mapping function is later employed during reconstruction of 3D volumes from plenoptic images.

For application to a rotating field of view, a method was devised whereby the coordinate system of the calibration plate was rotated with its azimuth angle (ψ). As the azimuthal rotation is proportional to the

orientation of the field of view, assigned object-space coordinates of the calibration plate's feature points remain constant throughout its angular sweep. For example, Fig. 2(b) is imaged at an azimuth angle of $\psi \approx 40°$ after Fig. 2(a), therefore, the coordinate set (x, y) is rotated by ψ to become (x', y'). This procedure results in the calibration polynomial being a function of azimuth angle:

$$(s, t) = P(x', y', z, u, v, \psi) \tag{2}$$

Calibration of the dot card in 2(b) with rotational DLFC results in 2(c) whereby the dot card appears at the same position as 2(a) despite the azimuthal rotation increasing by $\psi \approx 40°$.

A fixed volume would only require one calibration file whereas a continuously rotating volume with a fine enough angular resolution would require hundreds. The impracticality of physically calibrating volumes at every unique azimuth angle is avoided by exploiting the relationship between the mapping function coefficients and the rotation of the field of view. It was found by imaging a calibration plate through a full revolution that, conveniently, this is a periodic relation meaning that as the mirror rotates and thus the field of view rotates, the coefficients of the mapping function vary sinusoidally, as seen in Fig. 4 which shows three examples of coefficients plotted at every 10° for 360°. Therefore, in the rotational implementation of DLFC, calibration images are acquired for volumes at relatively broad increments of azimuth angle and mapping functions are generated for any desired in-between angles using interpolation.
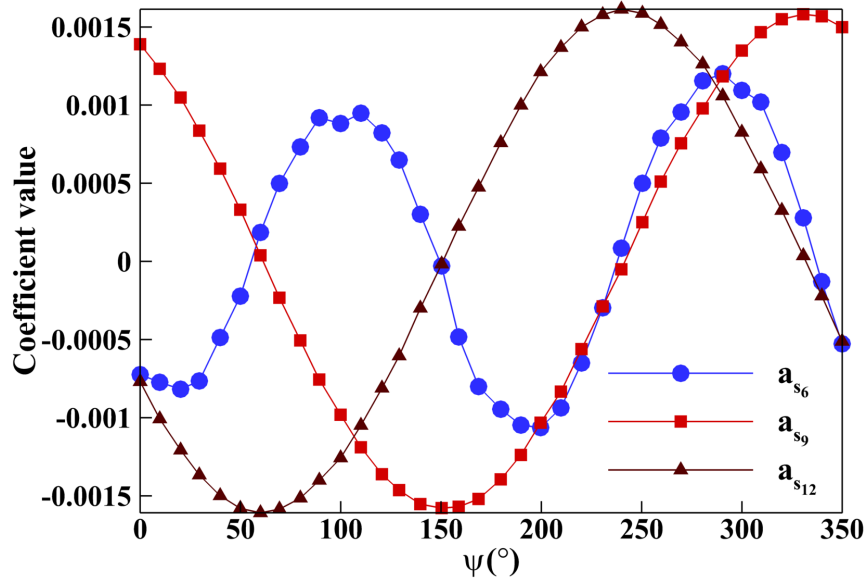

Figure 4: s-Coefficient values through a full revolution of calibration plate rotation (Gururaj et al. (2021))

A Fourier series was chosen as the most suitable representation of a periodic best fit curve and thus is used here to aid interpolation. Each mapping function coefficient was initially represented by a four-term Fourier series through its rotation:

$$(a_s, a_t) = f(\psi) = b_0 + \sum_{i=1}^{n} b_i cos(iw\psi) + c_i sin(iw\psi) \tag{3}$$

where w is a measure of the periodicity of a mapping function coefficient, n refers to the selected number of harmonics, and b and c are cosine and sine coefficients, respectively. If the four-term series was deemed to be overfitting the coefficients, the number of terms in the Fourier series was dropped to three and subsequently two if overfitting persisted. Goodness of fit was determined using a combination of the coefficient of determination (R^2) and a comparison of global absolute maxima between the Fourier curve and known coefficients. In either case, a user-defined threshold was set, the violation of which resulted in sequentially dropping the number of harmonics. For the rotating experiments presented here, images of the calibration plate were captured across a depth of 81.28 mm at approximately every 10° increment for a total sweep of 90° while coefficients were interpolated for each intermediate angle at which flow images were acquired according to encoder outputs. For example, in the case of the lowest rotation rate wingless experiment,

982 mapping functions were generated with each corresponding to a different azimuth angle using just 10 physically calibrated volumes.

In summary, the rotational DLFC technique involves acquiring images of a calibration plate at discrete yet widely spaced azimuth angles across multiple depths throughout an angle sweep that encompasses the relevant range of rotation of the wing. A mapping function is generated at each of these angles by applying a generic third-order polynomial to the image and object space coordinates of known calibration points via discretized perspective views. Coefficients for any angle within the swept range of the calibration plate are interpolated for using a fitted Fourier series. This mapping function is then employed during reconstruction meaning the calibrated volume at each azimuth angle is mapped to a common set of in-plane coordinates (x', y') thus eliminating the effects of the rotating field of view when tracing particles into the volume.

A reprojection error analysis was performed for the physically calibrated volumes in R3DV. As a measure of comparison, the same camera configuration was used to calibrate a stationary volume on a benchtop setup. In the latter, a 300 mm Thorlabs motorized translation stage was used to provide positioning of the calibration plate with a precision of 0.5 μm. Reprojection error was calculated by applying the corresponding mapping function to known calibration plate feature points in object space (x, y, z) to solve for (s_{reproj}, t_{reproj}), the reprojected image space position. This was compared to (s, t), considered the true image space location, for each feature point. Resulting pixel values were then scaled with respect to the plenoptic camera's perspective view resolution. In the rotational case, no trend in the reprojection error was observed with respect to varying azimuth angles. Averaged across all 10 azimuth angles, the errors in rotational DLFC applied with the R3DV setup as well as the benchtop conditions are shown in Table 1. For R3DV, an increase in reprojection error of $\sim$0.15 occurs in the s-direction while the t-axis holds a $\sim$0.3 increase. Possible factors contributing to this rise include needing to image through a much thicker acrylic wall using the R3DV setup relative to the benchtop as well as imperfections in R3DV's 3D-printed calibration mounting wing. The error in rotational calibration did not show a consistent dependency on ψ. Whilst the comparison suggests the rotational calibration configuration has potential for improvements, subpixel accuracy is still obtained and, as section 4 will show, the overall measurement uncertainty of the technique is on par with stationary plenoptic-PIV. Therefore, the higher error of R3DV's calibration is considered acceptable albeit a task for future work to reduce.

Table 1: Reprojection errors of R3DV's rotational DLFC versus conventional DLFC on benchtop setup

Setup	Reprojection error (px)	
	s	t
R3DV	0.413	0.590
Benchtop	0.259	0.286

4 Uncertainty Analysis

In order to quantify uncertainty of the velocity vector fields, images of quiescent flow were acquired via the mirror undergoing steady rotation. Cross-correlation was performed on these images to generate vectors of velocities that represent the displacement in particle position due solely to imaging via the rotating mirror. The initial vectors output in the camera's rectangular coordinate system were transformed to a cylindrical frame (Fig. 5) for convenience as follows:

$$u_t = u\cos\theta + w\sin\theta \tag{4}$$

$$u_v = v \tag{5}$$

$$u_r = w\cos\theta - u\sin\theta \tag{6}$$

$$R' = \frac{R}{cos\theta} \tag{7}$$

$$\theta = \tan^{-1}\left(\frac{x - x_0}{R}\right) \tag{8}$$

where u, v, and w are velocities in the horizontal, vertical, and depth directions of the raw cross-correlated vectors, respectively. Similarly, u_t, u_v, and u_r are velocities in the tangential, vertical, and radial directions, respectively, in relation to the cylindrical path of rotation.
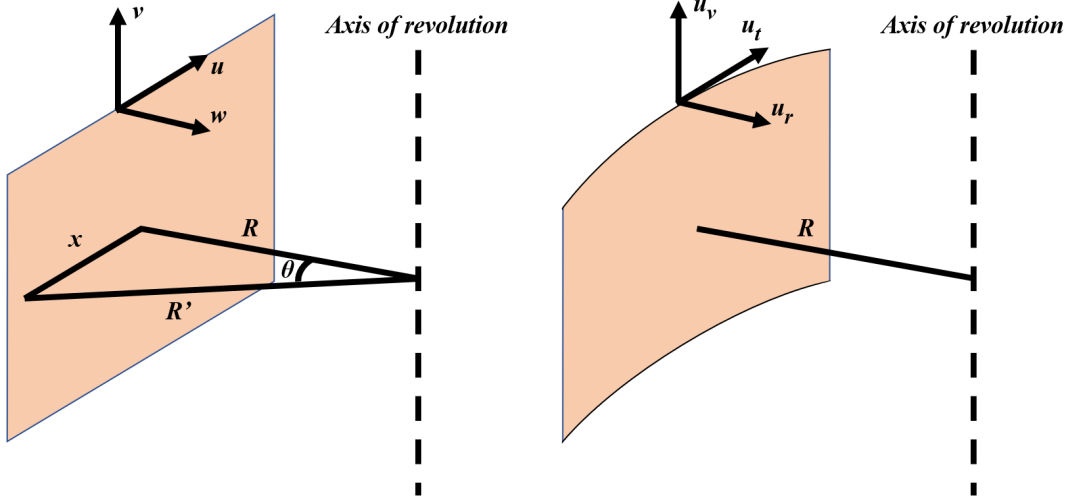

Figure 5: Schematic of coordinate transformation from Cartesian (left) to cylindrical (right)

In quantifying uncertainty, vector fields were compared to a model described by rotational kinematics:

$$u_t = \Omega_{rot} R = \Omega_{rot}(r - R_0) \tag{9}$$

$$u_v = 0 \tag{10}$$

$$u_r = 0 \tag{11}$$

where Ω_{rot} is the rotation rate and r is measured relative to R_0, the radial distance from the center of rotation to the calibrated center plane. While the location of the in-plane center of rotation, x_0, is not known from physical parameters, it can be calculated using rotating images of the calibration board as follows. When assigning object space positions to feature points during DLFC, $(0, 0)$ is chosen arbitrarily as long as it remains consistent to the same feature throughout every calibration image. The objective now becomes to find the distance of the center of rotation to the calibrated $(0, 0)$. This can be achieved by tracking the position of a feature point through a series of images following the rotation of the calibration plate. A least-squares algorithm is then used to fit a circle to the positions of the rotating dot in order to find its center of rotation (Pratt (1987)). Finally, the known image magnification is applied to back out x_0, the object-space distance of the in-plane center of rotation to the calibrated center position. Ω_{rot} and R_0 are estimated through a Levenberg-Marquardt least-squares minimization of velocity vectors after substituting Eq. (4) into Eq. (9).

Comparison of the model (Fig. 6(a)) to the time-average of the steady-state portion of wingless motion (Fig. 6(b)) was determined to give the systematic error in assuming purely rotational motion, $\Delta \overline{u}$. Note the velocity close to the edges of Fig. 6(b) drops towards 0 due to this portion of the volume being outside the field of view across most azimuth angles. On average, an error less than 1% of the tangential velocity occurred in the tangential direction, equivalent to less than 0.1 voxels per timestep. The model also assumed zero velocity in the vertical and radial directions. Here, the comparison yielded $\Delta \overline{u_v}$ and $\Delta \overline{u_r}$ less than 0.15 and 0.6 voxels per frame, respectively. Voxel error values far below average particle displacements in the direction of motion confirmed the PIV measurements obtained using this experimental setup could be accurately modeled by pure rotation. It was noted that the in-plane systematic error increased further from the center of the vector field. As an example, Fig. 7 plots the spatial variation of $\Delta \overline{u_t}$ normalized with respect to u_t for a portion of the center xy-plane of the RPM ≈ 1, volume 2 experimental configuration. No consistent relationship was found with respect to error across the depth direction.

After establishing that the system could be described by the rotational model, quantification of measurement uncertainty, $\delta u'$, was achieved by generating a model for the vector field at each azimuth angle, u'_{model}, and comparing velocities from the cross-correlated vectors (Fig. 6(c)) to their respective ideal values. The standard deviation of residual velocities from this comparison was taken as a value representative of measurement uncertainty. An experimental setup consisting of different imaging conditions at each azimuth
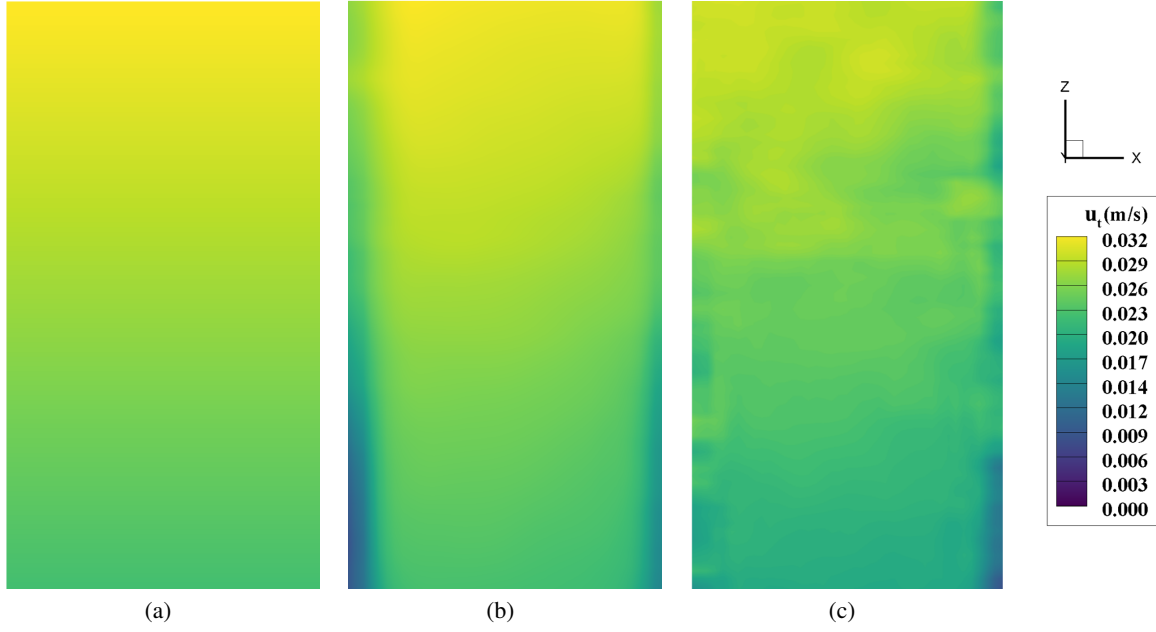
Figure 6: Example of an instantaneous R3DV vector field's velocity distribution (right) vs time-averaged vector field (center) and a corresponding idealized model (left) calculated based on rotational kinematics

angle begs the question as to whether uncertainty possesses a dependency on azimuth angle. Fig. 8 plots $\delta u_t'$ for a rotation of approximately 60° for volume 2 with the mirror rotating at approximately 5 RPM. Clearly, the uncertainty fluctuates randomly around 0.15. This randomness with azimuth angle was seen in all six test cases. Similarly, the $\delta u_r'$ and $\delta u_v'$ exhibit no relationship with azimuth angle. Accordingly, uncertainty was averaged across all azimuth angles for each volume and each rotation rate to yield a single value for the configurations shown in Table 2. Here, it is apparent the in-plane uncertainty is consistently higher for the farther volume 1. It was hypothesized this was caused by a slight increase in particle density across the two sets of experiments. Interestingly, volume 2 generally possesses a higher radial uncertainty. There also exists a slight trend of increasing tangential uncertainty with higher rotation rates, although in proportion to the mean tangential velocity it actually decreases. Due to the limited angular range of perspectives a plenoptic camera can obtain, particle elongation is always expected to cause reduced depth precision relative to that of the in-plane directions in a single-camera plenoptic experiment and this is certainly observed in Table 2. Overall, the authors assert the uncertainty for the current implementation of R3DV is less than 0.21 voxels per timestep for the in-plane components and better than 1.7 voxels per timestep in the radial direction. These values are comparable to those obtained by Fahringer et al. who determined the uncertainty of single-camera plenoptic-PIV in a stationary reference frame to be accurate to within 0.2 voxels and 1 voxel in the lateral and depth directions, respectively (Fahringer et al. (2015)).

5   Conclusions

The R3DV technique possesses unique challenges associated with imaging through a rotating mirror using a stationary camera, with one such challenge being an undesired rotation of the images recorded by the camera. The authors propose a rotational calibration method whereby the azimuth angle of the mirror is incorporated in the calibration function to rectify the rotating field of view to a common axis. Despite being higher than plenoptic calibration in a benchtop configuration, rotational DLFC's reprojection errors of less than 0.6 pixels were deemed acceptable for R3DV. A focus for future work will involve reducing this error by improving the physical design of the calibration plate mounting system. Quantification of uncertainty was achieved by comparing a model of rotation to vector fields obtained from quiescent flow viewed through a rotating mirror. The error in assuming the motion in the setup adheres purely to laws of rotational kinematics was first assessed and concluded to be insignificant. Comparison of instantaneous vector fields to their respective ideal models yielded average uncertainties better than 0.21 and 1.7 voxels per
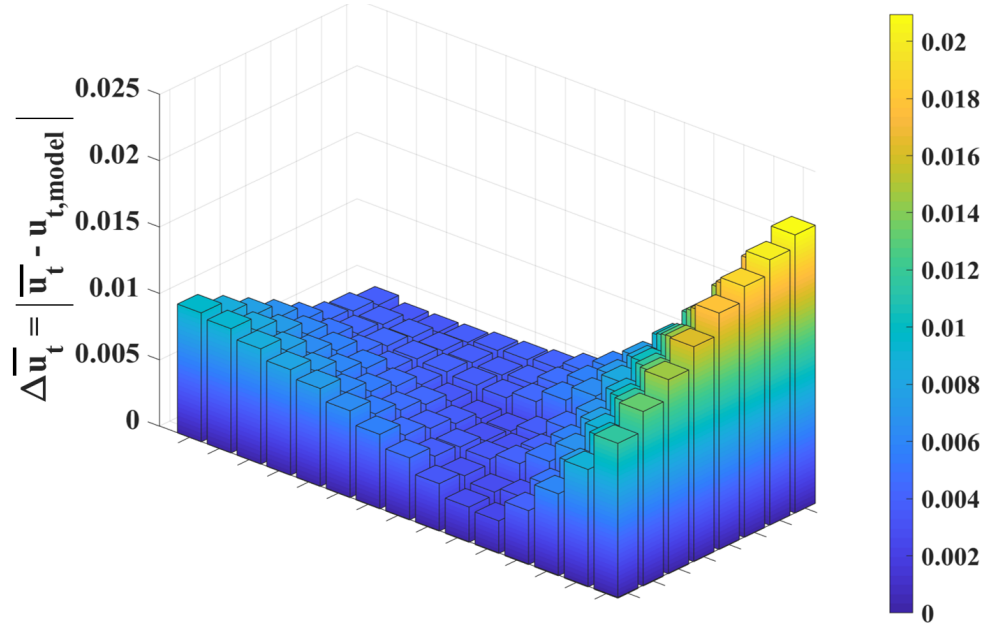
Figure 7: Spatial variation of systematic error in u_t normalized with respect to the model u_t across an xy-plane of volume 2, RPM ≈ 1
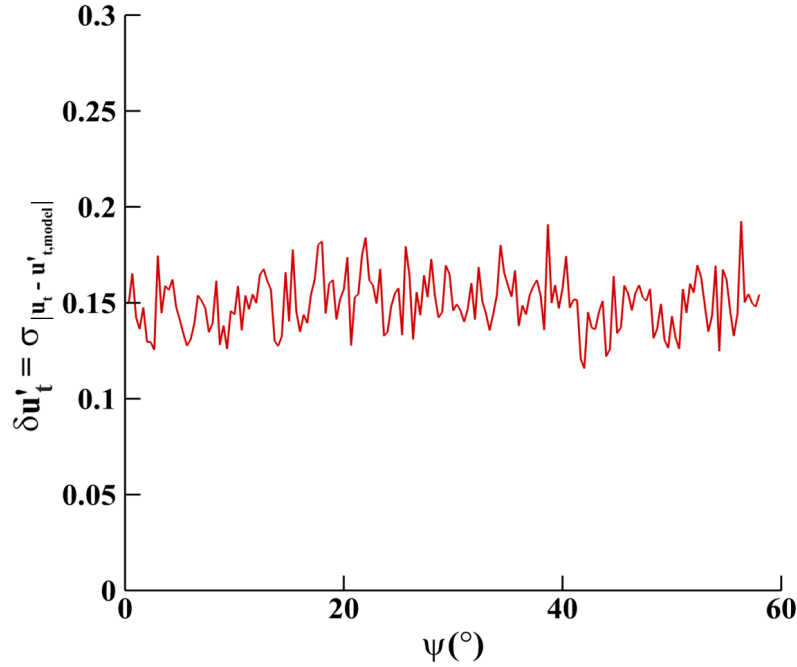

Figure 8: Variation of uncertainty in tangential velocity across a 60° azimuthal rotation

timestep in the in-plane and out-of-plane directions, respectively, each with no reliance on azimuth angle. As these values proved comparable to those found in previous work on plenoptic-PIV uncertainty estimation, the current implementation of R3DV is seen to be a success. Optimization of cross-correlation parameters is currently being explored with the aim of reducing uncertainty. Possibilities of future developments include implementing particle tracking velocimetry via the plenoptic ray-bundling triangulation method developed by Clifford et al. (2019) as well as investigating the fluid-structure interaction behavior of a rotor during the LEV life cycle.

Table 2: Average measurement uncertainty across six wingless R3DV experiments

Volume	Approximate rotation rate (RPM)	Uncertainty (voxels per frame)		
		$\Delta u'_t$	$\Delta u'_r$	$\Delta u'_v$
1	1	0.17	1.51	0.21
	3	0.18	1.47	0.20
	5	0.20	1.60	0.21
2	1	0.13	1.61	0.14
	3	0.14	1.66	0.15
	5	0.15	1.58	0.15

Acknowledgements

References

Clifford C, Tan ZP, Hall EM, and Thurow BS (2019) Particle matching and triangulation using light-field ray bundling. in CJ Kähler, R Hain, S Scharnowski, and T Fuchs, editors, *Proceedings of the 13th International Symposium on Particle Image Velocimetry*

Elsinga GE, Scarano F, Wieneke B, and van Oudheusden BW (2006) Tomographic particle image velocimetry. *Experiments in fluids* 41:933–947

Fahringer TW, Lynch KP, and Thurow BS (2015) Volumetric particle image velocimetry with a single plenoptic camera. *Measurement Science and Technology* 26:115201

Gururaj A, Moaven M, Tan ZP, Thurow B, and Raghav V (2021) Rotating three-dimensional velocimetry. *Experiments in Fluids*

Hall EM, Fahringer TW, Guildenbecher DR, and Thurow BS (2018) Volumetric calibration of a plenoptic camera. *Appl Opt* 57:914–923

Mulleners K, Kindler K, and Raffel M (2012) Dynamic stall on a fully equipped helicopter model. *Aerospace Science and Technology* 19:72–76

Percin M and Oudheusden BW (2015) Three-dimensional flow structures and unsteady forces on pitching and surging revolving flat plates. *Experiments in Fluids* 56:1–19

Pratt V (1987) Direct least-squares fitting of algebraic surfaces. *SIGGRAPH Comput Graph* 21:145–152

Tan ZP, Johnson K, Clifford C, and Thurow BS (2019) Development of a modular, high-speed plenoptic-camera for 3d flow-measurement. *Opt Express* 27:13400–13415